A Smart E-Scooter with Embedded Estimation of Rear Vehicle Trajectories for Rider Protection

Hamidreza Alai [a], Woongsun Jeon [b], Lee Alexander [a] and Rajesh Rajamani [a] *

[a] Department of Mechanical Engineering, University of Minnesota, Twin Cities, MN 55455, USA

[b] School of Electrical and Electronics Engineering, Chung-Ang University, Seoul 06974, South Korea.

Key Words: electric scooters, active sensing, collision prediction, vehicle detection, estimation, vehicle tracking, vehicle safety

* Corresponding author, rajamani@umn.edu, tel: 612-626-7961, 111 Church Street SE, Minneapolis, MN 55455, USA.

Nomenclature

c : number of failed detections in "target vehicle detection" algorithm

CoG: center of gravity of vehicle

D: feedforward noise matrix

E: state coefficient matrix

$\boldsymbol{f}(.)$: nonlinear state dynamics

$f_x(.)$: vehicle motion model corresponding to x

$f_y(.)$: vehicle motion model corresponding to y

$\hat{\boldsymbol{f}}(.)$: estimated nonlinear dynamics

$\tilde{\boldsymbol{f}}(.)$: error of estimated nonlinear dynamics

$\boldsymbol{g}(.)$: nonlinear input- state dynamics

H: output state matrix

I : identity matrix with proper dimension

k : coefficient in nonlinear model of system

l: wheelbase length of vehicle

l_f: vehicle front length

l_r: vehicle rear length

L: observer gain matrix

N_{min}: minimum number of points within minimum radius in DBSCAN algorithm

P: positive definite matrix in Lyapunov function

q: weight vector used to build Q

Q: weight matrix in H_∞ constraint

R: defined variable in LMI problem

$\boldsymbol{u}$: input vector of the system

u_k: input for stepper motor control

U, V: lower bound and upper bounds of Jacobian matrix of nonlinear state dynamics

V: velocity of vehicle

V_1: negative semi-definite term used in S- procedure lemma

$\boldsymbol{w}$: measurement noise

$\boldsymbol{x}$: states of system

$\hat{\boldsymbol{x}}$: estimated states of system

$\tilde{\boldsymbol{x}}$: error of estimated states of system

$\bar{\boldsymbol{x}}$: value between the true state value $\boldsymbol{x}$ and estimated state value $\hat{\boldsymbol{x}}$

X, x: relative longitudinal position of vehicle from e-scooter

$\boldsymbol{y}$: output vector of the system

Y, y: relative lateral position of vehicle from e-scooter

z_k: range measurement from laser sensor

β: vehicle slip angle

δ_F: steering angle of vehicle

δ_x: distance margin corresponding to x used for $ratio_{ref}$ calculation

δ_y: distance margin corresponding to y used for $ratio_{ref}$ calculation

ϵ: positive coefficient used in S- procedure lemma

μ: coefficient in H_∞ constraint

ρ: minimum radius in DBSCAN algorithm

Φ_k: orientation angle laser sensor (stepper motor)

Φ_{max}: maximum orientation angle for stepper motor

Φ_{min}: minimum orientation angle for stepper motor

ψ: yaw angle of vehicle

Ω: matrix used in negative semi-definite term V_1

Abstract

This paper develops an active sensing and estimation system for protecting the rider of an e-scooter from car-scooter collisions. The objective is to track the trajectories of cars behind the e-scooter and predict any real-time danger of car-scooter collision. If the danger of a collision is predicted, then a loud car-horn-like audio warning is sounded to alert the car driver to the presence of the scooter. A low-cost (~$100) single-beam laser sensor is chosen for measuring the positions of cars behind the scooter. The sensor is mounted on a stepper motor and the region behind the scooter is scanned to detect vehicles. Once a vehicle is detected, its trajectory is tracked in real-time by using feedback control to focus the orientation of the laser sensor such as to make measurements of the right front corner of the vehicle. A nonlinear vehicle model and a nonlinear observer are used to estimate the trajectory variables of the tracked car. The estimated states are used in a receding horizon controller that controls the real-time position of the laser sensor to focus on the vehicle. The developed system is implemented on a Ninebot e-scooter platform. Extensive experiments conducted with multiple vehicle maneuvers show that the closed-loop system is able to accurately track vehicle trajectories and provide audio alerts to prevent collisions. This paper constitutes the first-ever development of active rider protection technology for the protection of e-scooters.

1. Introduction

Over the last seven years, standing electric scooters have proliferated rapidly as an inexpensive and easily available mode of transportation. A market research company has predicted e-scooters will grow from a US$14 billion global market in 2014 to $37 billion in 2024 [1]. Bird and Lime, the two largest shared scooter operators, have placed scooters in a large number of cities across the U.S.. Scooters serve as an alternate to ride-sharing and public transit and provide personal pleasure to many commuters. They are described as “micro-mobility” which provides the last-mile commute or a full commute option for workers who live within a few miles of their workplace. Rules and regulations regarding the use of e-scooters vary widely with location and country [2]. In the US, scooters are typically not allowed on high-speed streets (> 35 mph) [4]. Some states do allow e-scooters to be operated on sidewalks while others specifically ban their use on sidewalks [3]. The use of bicycle lanes by e-scooters is explicitly allowed in some states but is not a part of explicit rules in others. The maximum allowed speed of operation again varies from state to state and can be as low as 15 mph [4]. Outside the US, countries that have regulations regarding the maximum speed, rider age and possible e-scooter license requirements include Singapore, Germany, France, UK, Australia and New Zealand [2].

Scooter riders constitute a vulnerable population on roads and are in significantly more danger of suffering from severe injuries and fatalities in any car-scooter collision (compared to the occupants of the car). There is limited crash data available on e-scooters, due to their relatively recent appearance as part of the commuting vehicle infrastructure. Injuries resulting from e-scooters typically include head injuries or injuries to upper or lower extremities and range from minor contusions or lacerations to severe fractures or hemorrhages [5]- [7]. While relatively few deaths have occurred on e-scooters (compared to overall traffic fatalities), some studies have specifically found car-scooter crashes to be the most significant cause of e-scooter rider fatalities [8]. There is inadequate statistically meaningful data available in US crash databases on e-scooter related crashes. However, researchers used media and police reports to create a crash dataset of rented e-scooter fatalities for the 2018-2019 period and identified 17 corresponding records from the National Highway Traffic Safety Administration data [9]. They found that compared to fatalities from other modes of transportation, e-scooter fatality victims are younger, with more fatalities occurring at night and with the highest proportion of alcohol involvement of any mode [9]. The findings of another study

from France [10] also suggest that trauma involving e-scooters in France has significantly increased over the past 4 years. These patients presented with injury profiles as severe as those of individuals who experienced bicycle or motorbike RTCs, with a higher proportion of severe traumatic brain injury.

A more comprehensive data analysis of hospital data by the US Consumer Product Safety Commission found that emergency room visits in the US surged 450% from 7,700 in 2017 to 42,200 in 2021, with these estimates likely being an undercount [11]. Similarly, as an international example, a retrospective review was performed of the medical records of patients seen from 2015 to 2016 at an emergency department (ED) in Singapore [12], to analyze scooter-related injuries. There was found to be a 2.3-fold increase in the number of scooter-rider severe injuries from 2015 to 2016. It should be noted that injury rates may differ between different generations of scooters.

Regarding cost estimates for e-scooter injuries, these vary greatly depending on the country [13]. However, these cost estimates focus solely on the cost of the hospital treatment [14], [15]. Economic impact on society from a broader perspective has not been studied in these references.

Unlike the inadequate analysis of crash data on e-scooters, there are many studies done to analyze crashes of bicycles with motor vehicles. Based on an Insurance Institute for Highway Safety (IIHS) study, 45% of the fatalities of bicycle crashes are in scenarios in which a vehicle is traveling in the same direction as the bicycle [16], suggesting that rear vehicle detection and tracking can be very helpful for the safety of bicycles or e-scooters. This also can be implied from another report and the citations in this report [17] showing that 40% of the collisions between bicycles and vehicles are rear-end. For this reason, our focus in this paper is to investigate a method for rear vehicle tracking to protect the e-scooter rider from vehicles that are approaching from behind the e-scooter.

The objective of the e-scooter protection system in this paper is to continuously track the trajectories of rear vehicles both directly behind and also in the adjacent lane next to the e-scooter's lane. If a danger of car-scooter collision is predicted, then a loud audio alert (a honk) is sounded to warn the car driver about the presence of the e-scooter. The tracking system is based on the use of a nonlinear observer and a low-cost sensor suitable for an e-scooter. The philosophy behind the approach is that the low-cost system can directly be sold to scooter riders and will be useful immediately on today's roads, since it does not require all the cars on the road to be equipped with new technology but relies on just the e-scooter itself for warning the car driver.

It should be noted that ADAS systems are being developed on new cars with various degrees of forward collision warning capabilities and utilize cameras, radar and sonar sensors [18], in addition to Lidar sensors on autonomous vehicles. While Lidar and radar sensors are significantly more expensive than the laser sensor utilized in this paper, sonar sensors have shorter range (of the order of 5 m) and cameras require significant computational power while not being robust to weather and lighting conditions. ADAS systems with pedestrian detection systems based on cameras are also becoming available [19]. However, the development of systems for bicycle and e-scooter detection are not widespread even on new automobiles and it will take many years for such technologies to become ubiquitous on all cars in the road.

To the best of this research team's knowledge, automotive companies and researchers have not focused on rear-vehicle tracking. There has not been adequate reason for automotive companies to detect the danger of collisions from vehicles behind an ego vehicle, such as being done in this paper – The active safety systems on vehicles are typically not concerned by vehicles behind the ego-vehicle and are not expected to react to them. On the other hand, vulnerable users like bicycles, pedestrians and e-scooters need to track vehicles behind them if these could pose a danger to them. In the case of bicycles, only a few research teams and one company have developed sensor systems for bicyclist safety. A magnetometer-based system

has been developed to identify dangerous locations to bicycles due to heavy automotive traffic [20]. A Rutgers University team has explored a rear-approaching vehicle detection system using computer vision techniques [21]. An undergraduate Northeastern University team explored a sonar sensor system to monitor vehicles at the rear and front of a bicycle [22]. Garmin has developed a rear-collision prevention system using radar [23]. Researchers have explored a laser-sensor-based bicycle protection system [24]. The sensor systems explored so far for bicycles have not used nonlinear observers for tracking, unlike the system being studied here for e-scooters.

In summary, the major technical contributions of the paper are as follows:

a) Development and use of a nonlinear observer for estimating the trajectories of rear vehicles.
b) Use of an active orientation control algorithm to focus a laser sensor on a corner of the rear vehicle, with the real-time orientation control of the laser sensor based on estimated states obtained from the nonlinear observer.
c) Presentation of an integrated algorithm to perform initial vehicle detection, followed by state estimation for vehicle tracking, and laser sensor orientation control for following the rear vehicle based on the estimated states of the nonlinear observer.
d) Implementation of the entire system on a prototype e-scooter with all of the algorithms implemented entirely on a Teensy microprocessor and all of the electronics contained installed compactly on the e-scooter.
e) Extensive experimental results evaluating the performance of the integrated system in tracking rear vehicles performing various types of maneuvers.

There has been significant recent interest in this journal (MSSP) in estimation of vehicle motion related variables using Kalman filters and other stochastic estimation algorithms. For instance, the mass of the vehicle is estimated based on longitudinal dynamic models and IMU/ GNSS measurements using a Kalman filter in [25]. Estimation of tire forces using a Kalman filter and a multi-body vehicle model is presented in [26]. The estimation of lateral and longitudinal vehicle velocities using a stochastic estimation algorithm and IMU/GNSS measurements is presented in [27]. Finally, road slope estimation based on an interactive multiple model algorithm in presented in [28]. The present paper differs from the above in its estimation approach by using a nonlinear observer instead of a stochastic estimation filter. One significant advantage of a nonlinear observer is its guaranteed global stability in the presence of nonlinear dynamics.

The outline of the paper is as follows. The rear vehicle detection system is described in section 2. The vehicle nonlinear model used for estimation is described in section 3. The nonlinear observer design and the associated LMI problem are described in sections 4 and 5. The controller design is described in section 6 and the simulation and experimental results are shown in section 7.

2. Rear Vehicle Detection

This section describes the vehicle detection algorithm using a low-cost laser sensor mounted on a stepper motor as shown in Fig. 1. Vehicle detection identifies whether or not measurements from an object behind the e-scooter are from a car. Vehicle detection is needed before vehicle tracking can be initiated. While 2-D and 3-D LIDAR sensors can provide detailed shapes of objects in the environment, their cost/size disadvantages make them an inappropriate choice for the e-scooter application. Hence, we are using a single-beam laser sensor with specifications mentioned in Table 1. The sensor was mounted at a height of 66 cm from the ground, nominally above the bumper height of a typical sedan (which is 40 – 50 cm). The sensor is low-cost (~$ 100) but has a single thin laser beam with a very narrow field of view, making it unable to view the full environment behind the e-scooter at once. Therefore, the laser sensor is mounted on

a stepper motor and is actively controlled to first scan and detect a vehicle and then subsequently track the vehicle continuously by closed-loop control of its orientation. While the range of the sensor is specified as 40 meters, the sensor was found in experiments to reliably detect all vehicles only at distances below 30 m.

Table. 1. Garmin LIDAR Sensor Specifications.

Sensor	Price	Range	Weight	Accuracy	Size
Garmin LIDAR-Lite v3	$129.99	5 cm- 40 m	22 g	±2.5 cm	40 × 48 × 20 mm

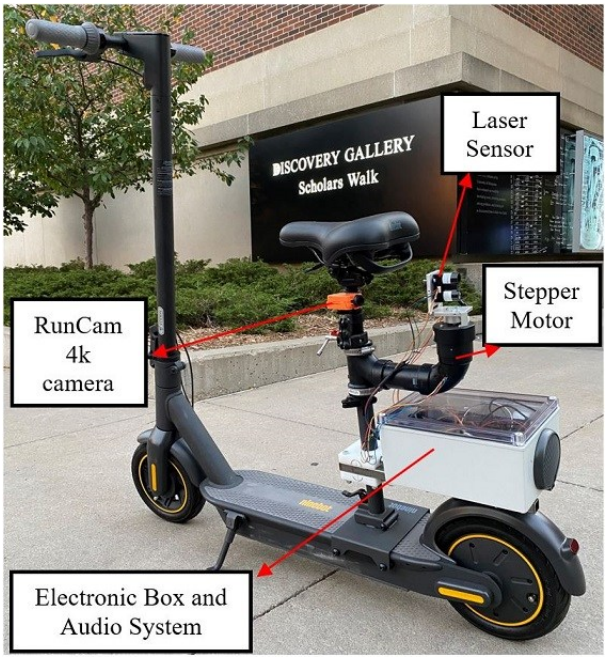

Fig. 1. Laser sensor system, audio system, and the camera on the Ninebot MAX e-Scooter.

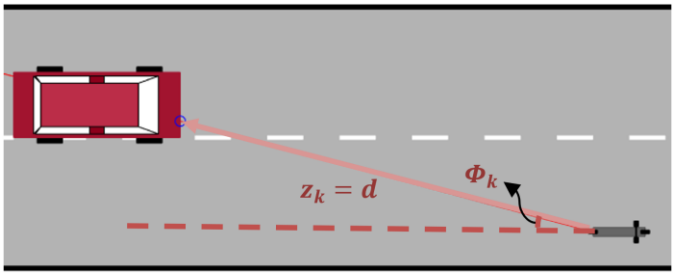

Fig. 2. Schematic of measurements from the system (angle and distance to the target are obtained when the laser sensor detects the object).

First, the rotational laser sensor scans the area of interest over a sweep angle of 30 degrees behind the e-scooter. Range measurements z_k at 100 Hz are obtained at different orientation angles Φ_k as shown in Fig. 2, by rotating the sensor in order to detect any rear-approaching vehicles. Measurements by the laser sensor need not be just from a car, but might be from objects such as road signs, road traffic barriers, trees, and parked cars. A clustering-based target detection algorithm is developed based on the measurement density and width for reliable detection of the target vehicle. The density-based spatial clustering of application with noise (DBSCAN) [29] algorithm is utilized for this purpose and customized for the E-

scooter application. DBSCAN identifies clusters by examining the local density of data in spatial data sets based on two pre-defined parameters: a minimum radius ρ and a minimum number of points within the radius N_{min}. The DBSCAN groups data points together as a cluster if, for each point of the cluster, the neighborhood of a given radius ρ contains at least minimum number of points N_{min}. The flowchart of the algorithm is shown in Fig. 3. The laser sensor system initially keeps scanning over a pre-determined range and stores measurements to an array. At each sampling time, DBSCAN is utilized on the stored measurement data and examines whether it constitutes a cluster or not. Measurement data from small objects or outliers will not contribute to the cluster if proper ρ and N_{min} values are chosen for the algorithm in the flow-chart. After the isolated cluster is found, the cluster is examined for its size and pattern of the data. From the cluster size, too large or too small an object, such as a building or a pedestrian, can be distinguished and separated from a vehicle. The data pattern of the cluster can also differentiate a rear-approaching vehicle from non-moving objects. For example, it cannot be an object approaching the e-scooter if the measurements (distance between the object and scooter) keep increasing. If the cluster is confirmed as an approaching vehicle, the sensor system reverses its scan direction to find the initial relative position between the scooter and the right-front corner position of the target vehicle. If the reversed scan direction is counter-clockwise, the sensor system scans over the target vehicle until the sensor misses and obtains no measurement from the target vehicle, in order to find the right front corner. Then, the last measurement from the target vehicle is utilized as the initial relative position of the target vehicle. If the reversed scan direction is clockwise, the sensor system scans until the sensor obtains the first measurement from the target vehicle and this measurement is then used as the initial relative position of the target vehicle. Finally, the target detection is completed, and the sensor system initiates its closed-loop tracking.

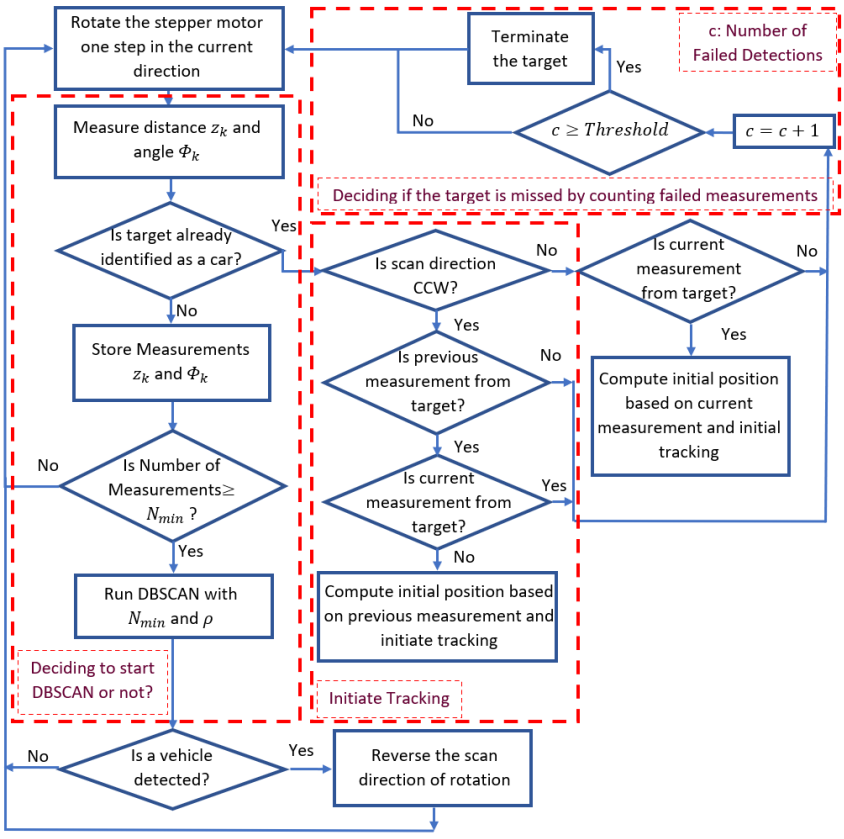

Fig. 3. Rear target detection based on the DBSCAN algorithm.

3. Vehicle Nonlinear Model

After detecting the presence of a vehicle behind the e-scooter, the single beam laser sensor should start tracking the position and orientation of the vehicle in order to predict any potential danger of collision. Thus, it is required that the system continuously estimate the trajectory of the detected vehicle. In this section, a nonlinear bicycle model of a vehicle is presented which will be used for the development of the nonlinear observer in the next section. Fig. 4 shows a vehicle with the total velocity of V (at the Center of Gravity or CoG), yaw angle of ψ, and steering angle of δ_F.

Assuming that the reference coordinate system is attached to the sensor location of the e-scooter as shown in Fig. 2, X and Y represent the relative position of the vehicle from the e-scooter. Assuming constant velocity, the state and output vectors are defined as:

$$\boldsymbol{x} = [X \quad Y \quad \psi \quad \delta_F]^T \quad \text{and} \quad \boldsymbol{y} = [X \quad Y]^T \tag{1}$$

The nonlinear model of the vehicle can be described as [30]:

$$\dot{\boldsymbol{x}} = \begin{bmatrix} \dot{X} \\ \dot{Y} \\ \dot{\psi} \\ \dot{\delta}_F \end{bmatrix} = \begin{bmatrix} V\cos(\psi+\beta) \\ V\sin(\psi+\beta) \\ V\cos\beta\ \tan\delta_F/\ell \\ 0 \end{bmatrix} \tag{2}$$

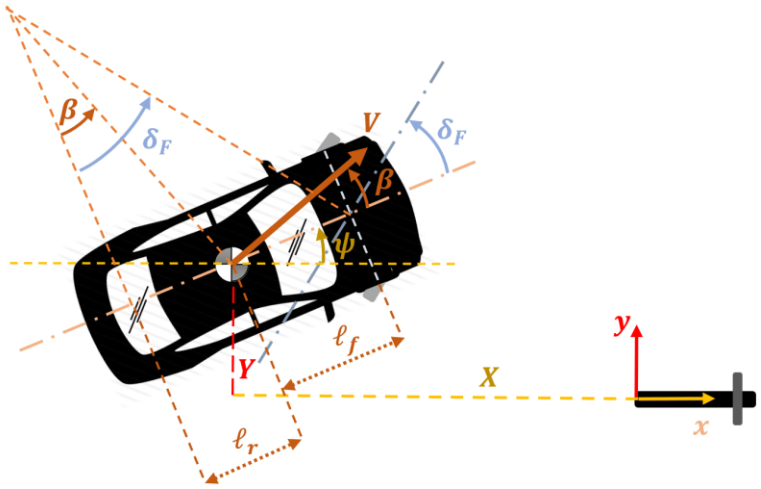

Fig. 4. Vehicle motion schematic and model variables

The parameter $l = l_f + l_r$ is the wheelbase length of the vehicle and $\beta = tan^{-1}\left(l_r \frac{tan(\delta_f)}{l_f+l_r}\right)$. The vehicle model can be represented in the following general form:

$$\dot{\boldsymbol{x}} = k\boldsymbol{f}(\boldsymbol{x}) + \boldsymbol{g}(\boldsymbol{y},\boldsymbol{u}) = \begin{Bmatrix} kf_1(E_1\boldsymbol{x}) \\ \vdots \\ kf_n(E_n\boldsymbol{x}) \end{Bmatrix} + \boldsymbol{g}(\boldsymbol{y},\boldsymbol{u})$$
$$\boldsymbol{y}(\boldsymbol{x}) = H\boldsymbol{x} + D\boldsymbol{w} \tag{3}$$

where $\boldsymbol{x} \in R^n, \boldsymbol{y} \in R^m, \boldsymbol{u} \in R^p, k = V \in R$, $E_i^T \in R^n, H \in R^{m \times n}, D \in R^{m \times q}$, $f_i: R \to R$, $i = 1,2,\dots,n$, $\boldsymbol{g}(\boldsymbol{y}, \boldsymbol{u})$ is $R^{m\,x\,p} \to R^n$, and $\boldsymbol{w} \in R^q$ is measurement noise. The variable $E_i \boldsymbol{x}$ is a linear scalar combination of the states.

It should be noted that slip angle at the CoG of the vehicle is utilized but the use of tire forces in which the tire force varies as a function of the slip angle is avoided. This is because such a model becomes a function of a large number of tire and vehicle parameters. Since the vehicle that is encountered is unknown, the values of these parameters cannot be known. Hence, the above model that includes vehicle slip angle is more appropriate, in spite of not involving slip angles at the tires.

For the vehicle model (2), the general system (3) will be simplified as:

$$\begin{gathered} \boldsymbol{g}(\boldsymbol{y}, \boldsymbol{u}) = 0 \\ f_1 = \cos\psi\,, f_2 = \sin\psi\,, f_3 = \tan\delta_F\,/l\,, f_4 = 0 \\ H = \begin{bmatrix} 1 & 0 & 0 & 0 \\ 0 & 1 & 0 & 0 \end{bmatrix} \\ E_1 = E_2 = [0\ 0\ 1\ 0], E_3 = [0\ 0\ 0\ 1], E_4 = [0\ 0\ 0\ 0] \end{gathered} \tag{4}$$

The arguments of the nonlinear functions $f_i\,(E_i x)$ in the general formulation (3) are a linear scalar combination of the states. Let $\tilde{\boldsymbol{f}} = \boldsymbol{f} - \hat{\boldsymbol{f}}$ where $\hat{\boldsymbol{f}} = \boldsymbol{f}(\hat{\boldsymbol{x}})$. Then from the differential mean value theorem (DMVT):

$$\tilde{f}_i = f_i - \hat{f}_i = \left.\frac{\partial f_i}{\partial (E_i x)}\right|_{x=\bar{x}} E_i \tilde{x}$$

Hence

$$\tilde{\boldsymbol{f}} = \boldsymbol{f} - \hat{\boldsymbol{f}} = \begin{bmatrix} \left.\frac{\partial f_1}{\partial (E_1 \boldsymbol{x})}\right|_{\boldsymbol{x}=\bar{\boldsymbol{x}}} & \cdots & 0 \\ \vdots & \ddots & \vdots \\ 0 & \cdots & \left.\frac{\partial f_n}{\partial (E_n \boldsymbol{x})}\right|_{\boldsymbol{x}=\bar{\boldsymbol{x}}} \end{bmatrix} E\tilde{\boldsymbol{x}} \tag{5}$$

where $\bar{\boldsymbol{x}}$ is a value between the true state value $\boldsymbol{x}$ and estimated state value $\hat{\boldsymbol{x}}$. Note that equation (5) is based on the DMVT, is exact for some $\bar{\boldsymbol{x}}$ and is not an approximation. Assume that the functions f_i have bounded Jacobians, namely let:

$$U_i \le \left.\frac{\partial f_i}{\partial (E_i \boldsymbol{x})}\right|_{\boldsymbol{x}=\bar{\boldsymbol{x}}} \le V_i, \qquad \text{for} \qquad i = 1,2,\dots,n \tag{6}$$

$$E = [E_1 \quad \dots \quad E_n]^T \tag{7}$$

$$U = \begin{bmatrix} U_1 & 0 & \cdots & 0 \\ 0 & U_2 & \cdots & 0 \\ \vdots & \vdots & \ddots & 0 \\ 0 & 0 & 0 & U_n \end{bmatrix}, V = \begin{bmatrix} V_1 & 0 & \cdots & 0 \\ 0 & V_2 & \cdots & 0 \\ \vdots & \vdots & \ddots & 0 \\ 0 & 0 & 0 & V_n \end{bmatrix} \tag{8}$$

Hence

$$U \leq \begin{bmatrix} \left.\frac{\partial f_1}{\partial (E_1 \boldsymbol{x})}\right|_{x=\bar{x}_1} & \cdots & 0 \\ \vdots & \ddots & \vdots \\ 0 & \cdots & \left.\frac{\partial f_n}{\partial (E_n \boldsymbol{x})}\right|_{x=\bar{x}_n} \end{bmatrix} \leq V \tag{9}$$

The nonlinear observer in section 4 is designed based on the general form of the vehicle model (3) and the Jacobian bounds (9).

4. Nonlinear Observer Design

It is necessary to estimate the position and orientation of the rear vehicle so as to estimate its real-time trajectory. The estimated state values can then be used to control the stepper motor to point the laser beam at the right corner of the vehicle. The steps of the nonlinear observer design for this estimation task are described in this section. The active control of the laser beam orientation angle based on the estimated states is presented subsequently in section 5.

4.1. The Observer Design Formulation

The nonlinear observer for the system (3) is defined as in equation (10).

$$\dot{\hat{\boldsymbol{x}}} = k\boldsymbol{f}(\hat{\boldsymbol{x}}) + \boldsymbol{g}(\boldsymbol{y}, \boldsymbol{u}) + L[\boldsymbol{y} - H\hat{\boldsymbol{x}}] \tag{10}$$

Let the estimated error be given by:

$$\tilde{\boldsymbol{x}} = \boldsymbol{x} - \hat{\boldsymbol{x}} \tag{11}$$

Then taking the derivative of equation (11):

$$\begin{aligned} \dot{\tilde{\boldsymbol{x}}} &= \big(k\boldsymbol{f}(\boldsymbol{x}) + \boldsymbol{g}(\boldsymbol{y}, \boldsymbol{u})\big) - \big(k\boldsymbol{f}(\hat{\boldsymbol{x}}) + L[\boldsymbol{y} - H\hat{\boldsymbol{x}}] + \boldsymbol{g}(\boldsymbol{y}, \boldsymbol{u})\big) \\ &= k\tilde{\boldsymbol{f}}(\boldsymbol{x}, \hat{\boldsymbol{x}}) - L[H\boldsymbol{x} + D\boldsymbol{w} - H\hat{\boldsymbol{x}}] = k\tilde{\boldsymbol{f}}(\boldsymbol{x}, \hat{\boldsymbol{x}}) - LH\tilde{\boldsymbol{x}} - LD\boldsymbol{w} \end{aligned} \tag{12}$$

The estimated error $\tilde{\boldsymbol{x}}$ should converge to zero in the absence of sensor noise. It is also desired to have a H_∞ constraint on the estimation errors for sensor noise rejection:

$$\int_0^\infty \tilde{\boldsymbol{x}}(\boldsymbol{t})^{\boldsymbol{T}} Q \tilde{\boldsymbol{x}}(\boldsymbol{t}) dt \leq \mu \int_0^\infty \boldsymbol{w}(t)^T \boldsymbol{w}(t) dt \tag{13}$$

Define the following matrix to be used in Lemma 1:

$$\Omega = \begin{bmatrix} \frac{E^T U^T V E + E^T V^T U E}{2} & -\frac{E^T U^T + E^T V^T}{2} & 0 \\ -\frac{VE + UE}{2} & I & 0 \\ 0 & 0 & 0 \end{bmatrix} \tag{14}$$

***Lemma 1*:** The difference function $\tilde{\boldsymbol{f}}$ satisfies the following quadratic inequality based on the Jacobian bounds of f:

$$V_1 = [\tilde{\boldsymbol{x}}^{\boldsymbol{T}} \quad \tilde{\boldsymbol{f}}^{\boldsymbol{T}} \quad \boldsymbol{w}^T]\, \Omega \begin{bmatrix} \tilde{\boldsymbol{x}} \\ \tilde{\boldsymbol{f}} \\ \boldsymbol{w} \end{bmatrix} \leq 0 \tag{15}$$

Note that $\Omega < 0$ is a sufficient but not a necessary condition for (15). This is because $\tilde{\boldsymbol{f}}$ is itself a function of $\tilde{\boldsymbol{x}}$.

Proof: The following equations are obtained from equation (5) and inequality (9):

$$\begin{aligned} \tilde{\boldsymbol{f}} - UE\tilde{\boldsymbol{x}} &= diag\left\{ \frac{\partial f_1}{\partial(E_1\boldsymbol{x})}\Big|_{x=\bar{x}_1} - U_1, \dots\dots, \frac{\partial f_n}{\partial(E_n\boldsymbol{x})}\Big|_{x=\bar{x}_n} - U_n \right\} \\ \tilde{\boldsymbol{f}} - VE\tilde{\boldsymbol{x}} &= diag\left\{ \frac{\partial f_1}{\partial(E_1\boldsymbol{x})}\Big|_{x=\bar{x}_1} - V_1, \dots\dots, \frac{\partial f_n}{\partial(E_n\boldsymbol{x})}\Big|_{x=\bar{x}_n} - V_n \right\} \end{aligned} \tag{16}$$

It follows that:

$$\begin{cases} \left(\tilde{\boldsymbol{f}} - UE\tilde{\boldsymbol{x}}\right)^T \left(\tilde{\boldsymbol{f}} - VE\tilde{\boldsymbol{x}}\right) \leq 0 \\ \left(\tilde{\boldsymbol{f}} - VE\tilde{\boldsymbol{x}}\right)^T \left(\tilde{\boldsymbol{f}} - UE\tilde{\boldsymbol{x}}\right) \leq 0 \end{cases} \tag{17}$$

$$\Rightarrow \begin{cases} \tilde{\boldsymbol{f}}^T\, \tilde{\boldsymbol{f}} - \tilde{\boldsymbol{x}}^T E^T U^T \tilde{\boldsymbol{f}} - \tilde{\boldsymbol{f}} VE\tilde{\boldsymbol{x}} + \tilde{\boldsymbol{x}}^T E^T U^T VE\tilde{\boldsymbol{x}} \leq 0 \\ \tilde{\boldsymbol{f}}^T\, \tilde{\boldsymbol{f}} - \tilde{\boldsymbol{x}}^T E^T V^T \tilde{\boldsymbol{f}} - \tilde{\boldsymbol{f}} UE\tilde{\boldsymbol{x}} + \tilde{\boldsymbol{x}}^T E^T V^T UE\tilde{\boldsymbol{x}} \leq 0 \end{cases} \tag{18}$$

$$\Rightarrow \tilde{\boldsymbol{f}}^T\, \tilde{\boldsymbol{f}} - \frac{\tilde{\boldsymbol{x}}^T E^T U^T \tilde{\boldsymbol{f}} + \tilde{\boldsymbol{x}}^T E^T V^T \tilde{\boldsymbol{f}}}{2} - \frac{\tilde{\boldsymbol{f}} VE\tilde{\boldsymbol{x}} + \tilde{\boldsymbol{f}} UE\tilde{\boldsymbol{x}}}{2} + \frac{\tilde{\boldsymbol{x}}^T E^T U^T VE\tilde{\boldsymbol{x}} + \tilde{\boldsymbol{x}}^T E^T V^T UE\tilde{\boldsymbol{x}}}{2} \leq 0 \tag{19}$$

Writing the equation (19) in quadratic form:

$$V_1 = \begin{bmatrix} \tilde{\boldsymbol{x}}^{\boldsymbol{T}} \\ \tilde{\boldsymbol{f}}^{\boldsymbol{T}} \\ \boldsymbol{w}^T \end{bmatrix}^T \begin{bmatrix} \frac{E^T U^T VE + E^T V^T UE}{2} & -\frac{E^T U^T + E^T V^T}{2} & 0 \\ -\frac{VE + UE}{2} & I & 0 \\ 0 & 0 & 0 \end{bmatrix} \begin{bmatrix} \tilde{\boldsymbol{x}} \\ \tilde{\boldsymbol{f}} \\ \boldsymbol{w} \end{bmatrix} \leq 0 \tag{20}$$

Thus, V_1 is negative semi-definite [34].

■

***Theorem 1*:** If there exists a feasible solution consisting of observer gain L and $P > 0$ for the LMI (21), that gain L will make the observer (10) globally exponentially stable, while satisfying disturbance rejection constraint (13).

$$\begin{bmatrix} G & Pk + \epsilon\frac{E^T U^T + E^T V^T}{2} & -PLD \\ kP + \epsilon\frac{VE + UE}{2} & -\epsilon I & 0 \\ -D^T L^T P & 0 & -\mu \end{bmatrix} \leq 0 \tag{21}$$

where:

$$G = -H^T L^T P - PLH - \epsilon \frac{E^T U^T V E + E^T V^T U E}{2} + Q$$

Proof: Consider the following Lyapunov function candidate:

$$V = \tilde{\boldsymbol{x}}^T P \tilde{\boldsymbol{x}}, P > 0 \tag{22}$$

In the presence of the disturbance $\boldsymbol{w}$:

$$\begin{aligned} \dot{V} = \dot{\tilde{\boldsymbol{x}}}^T P \tilde{\boldsymbol{x}} + \tilde{\boldsymbol{x}}^T P \dot{\tilde{\boldsymbol{x}}} &= \left(k\tilde{\boldsymbol{f}}(\boldsymbol{x}, \hat{\boldsymbol{x}}) - LH\tilde{\boldsymbol{x}} - LD\boldsymbol{w}\right)^T P \tilde{\boldsymbol{x}} + \tilde{\boldsymbol{x}}^T P \left(k\tilde{\boldsymbol{f}}(\boldsymbol{x}, \hat{\boldsymbol{x}}) - LH\tilde{\boldsymbol{x}} - LD\boldsymbol{w}\right) \\ &= k\tilde{\boldsymbol{f}}^T P \tilde{\boldsymbol{x}} + \tilde{\boldsymbol{x}}^T P k \tilde{\boldsymbol{f}} - \tilde{\boldsymbol{x}}^T H^T L^T P \tilde{\boldsymbol{x}} - \tilde{\boldsymbol{x}}^T PLH\tilde{\boldsymbol{x}} - \boldsymbol{w}^T D^T L^T P \tilde{\boldsymbol{x}} \\ &\quad - \tilde{\boldsymbol{x}}^T PLD\boldsymbol{w} \end{aligned} \tag{23}$$

In matrix form

$$\dot{V} = \begin{bmatrix} \tilde{\boldsymbol{x}} \\ \tilde{\boldsymbol{f}} \\ \boldsymbol{w} \end{bmatrix}^T \begin{bmatrix} -H^T L^T P - PLH & Pk & -PLD \\ kP & 0 & 0 \\ -D^T L^T P & 0 & 0 \end{bmatrix} \begin{bmatrix} \tilde{\boldsymbol{x}} \\ \tilde{\boldsymbol{f}} \\ \boldsymbol{w} \end{bmatrix} \tag{24}$$

For disturbance rejection constraint (13):

$$\dot{V} + \tilde{\boldsymbol{x}}^T Q \tilde{\boldsymbol{x}} - \mu \boldsymbol{w}^T \boldsymbol{w} < 0 \tag{25}$$

Hence in quadratic form

$$\dot{V} + \tilde{\boldsymbol{x}}^T Q \tilde{\boldsymbol{x}} - \mu \boldsymbol{w}^T \boldsymbol{w} = \begin{bmatrix} \tilde{\boldsymbol{x}} \\ \tilde{\boldsymbol{f}} \\ \boldsymbol{w} \end{bmatrix}^T \begin{bmatrix} -H^T L^T P - PLH + Q & Pk & -PLD \\ kP & 0 & 0 \\ -D^T L^T P & 0 & -\mu I \end{bmatrix} \begin{bmatrix} \tilde{\boldsymbol{x}} \\ \tilde{\boldsymbol{f}} \\ \boldsymbol{w} \end{bmatrix} < 0 \tag{26}$$

Using the S- procedure lemma [31], the LMI is obtained from $\dot{V} + \tilde{\boldsymbol{x}}^T Q \tilde{\boldsymbol{x}} - \mu \boldsymbol{w}^T \boldsymbol{w} \leq \epsilon V_1$ using (20) and (26):

$$\begin{bmatrix} -H^T L^T P - PLH + Q & Pk & -PLD \\ kP & 0 & 0 \\ -D^T L^T P & 0 & -\mu I \end{bmatrix} - \epsilon \begin{bmatrix} \frac{E^T U^T V E + E^T V^T U E}{2} & -\frac{E^T U^T + E^T V^T}{2} & 0 \\ -\frac{VE + UE}{2} & I & 0 \\ 0 & 0 & 0 \end{bmatrix} < 0 \tag{27}$$

which is the LMI design problem (21) specified in the theorem. ■

It should be noted that the inequality (21) involves the product term PL in which both P and L are solution variables. However, it is well known in the literature that (21) can be converted into an LMI by defining a new variable $R = PL$, solving for P and R, and then obtaining L using $L = P^{-1}R$. Since P is positive definite and invertible, L is guaranteed to exist once P and R are obtained.

4.2. Solving the LMI Problem for the Vehicle Model

In this section, the nonlinear observer gain L is obtained by solving LMI (21) for the vehicle nonlinear equations using the SEDUMI solver in MATLAB software. To have a feasible solution for the LMI problem, the following reasonable upper and lower bounds are used with the nominal vehicle velocity of 7.5 m/s:

$$-15° \leq \psi \leq 15°, -10° \leq \delta_F \leq 10° \tag{28}$$

The disturbance rejection factor is assumed to be $\mu = 0.15$. For disturbance rejection, the vector q is defined to calculate the weight matrix Q:

$$q = [1 \quad 1 \quad 0.1 \quad 0], Q = q^T q \tag{29}$$

To maintain feasibility for the LMI problem, the vector q is chosen to have some zero elements as shown in equation (29). This structure ensures that noise reduction has high priority for the location states and is less important for the angle states. The resulting observer gain for these values is:

$$L = \begin{bmatrix} 8.4358 & -0.8236 & -0.8797 & -0.6744 \\ 1.1103 & 15.7523 & 19.0477 & 13.2052 \end{bmatrix}^T \tag{30}$$

The nonlinear observer (10) with the gain (30) is used for real-time vehicle trajectory estimation.

5. Tracking and Active Control

This section deals with the active control of the laser sensor system for continuous tracking of the rear vehicle. We aim to track the right front corner of the target vehicle by measuring alternately distances to the front and side of the vehicle at points close to the right front corner, since tracking this corner provides both lateral and longitudinal distance information. Therefore, the reference point for orientation control is changed alternately depending on the corresponding selection of which information (longitudinal or lateral) is needed. The receding horizon controller is used to determine the optimal control input to track the desired reference based on the predicted future vehicle motion under control input constraints considered in the receding horizon controller. The following optimization problem is therefore constructed for the sensor orientation control:

$$\begin{aligned} &\arg \min_{u_k} \left\| ratio_{\,ref} - \tan(\Phi_k + u_k) \right\|^2 \\ &ratio_{\,ref} = \begin{cases} \dfrac{\hat{y}_{k+1} + \delta_y}{\hat{x}_{k+1}} : longitudinal\ distance\ desired \\ \dfrac{\hat{y}_{k+1}}{\hat{x}_{k+1} + \delta_x} : lateral\ distance\ desired \end{cases} \\ &\text{subject to} \quad \hat{x}_{k+1} = f_x(X_k), \ \ \hat{y}_{k+1} = f_y(X_k), \\ &\qquad\qquad\ \ \hat{y}_{k+1} > 0, \\ &\qquad\qquad\ \ u_k \in U, \ \ \Phi_{min} \le \Phi_k + u_k \le \Phi_{max} \\ &u_k \in U : possible\ inputs\ for\ the\ stepper\ motors \end{aligned} \tag{31}$$

where $f_x(\cdot)$ and $f_y(\cdot)$ are the vehicle motion model corresponding to x and y, respectively, δ_x and δ_y are distance margins which are used to construct reference points on the target vehicle (assumed to be 10 cm), U is a finite set of feasible control inputs (steps are {1°,1.5°,2°}), and ϕ_k is the sensor orientation at time k. The margins need to be small enough for fast measurement updates and large enough for robustness to deal with vehicle maneuver changes. Using (31), we track the right front corner (x, y) of the target vehicle by measuring alternately distances to the front and side of the vehicle at points close to the right front corner. The predicted vehicle motion $(\hat{x}_{k+1}, \hat{y}_{k+1})$ is calculated based on the nonlinear model (2). From (31), a desired orientation for the laser sensor system is determined at every sampling time instead of waiting for the end of an open-loop scan range. Once the vehicle moves out of the area of interest or passes the e-scooter (i.e., $\phi_k + u_k < \phi_{min}$ or $\phi_k + u_k > \phi_{max}$), the sensor system stops tracking and starts to search for a new target vehicle.

Whether a received reflection is from the front or side of a vehicle is determined by computing the slope of the line joining consecutive measurement points. If the slope of this line is small, it implies that the new reading has not switched from the front of the car to the side of the car, or vice versa. On the other hand, if the slope of this line is sufficiently big, then it implies that the new reading has switched from the front of the car to the side of the car (or vice versa). If no readings from the side of a vehicle are received, then the slope always indicates that the front of a vehicle is being measured, and the reading becomes zero when the laser sensor moves beyond the corner of the car without receiving any side readings. This is incorporated in our algorithm, since tracking a car right behind the e-scooter (where the side is not visible and no side reflections are received) is a very common scenario.

Measuring lateral and longitudinal distances alternately enables the closed-loop system to track the corner of the vehicle using the receding horizon controller and the nonlinear observer (10), in spite of using just a single beam laser sensor.

6. Simulations and Experiments

6.1. Simulation Results

To evaluate the tracking and estimation algorithms, we simulated the e-scooter and a vehicle in MATLAB with several different trajectories representing the four scenarios in Fig. 5, namely

a) vehicle travels right behind the e-scooter
b) vehicle travels adjacent to the e-scooter and then changes lanes to come behind the e-scooter
c) vehicle travels adjacent to the e-scooter
d) vehicle travels behind the e-scooter and changes lanes to come adjacent to the e-scooter.

Results of the MATLAB simulations are presented in Fig. 6. As shown in Fig. 6, the algorithm can track the vehicle and accurately estimate the states in the simulation for all 4 scenarios. The curve plotted with black circles shows the raw measurements from the laser sensor. The curve plotted with blue *'s shows the estimates from the nonlinear observer. In each of the 4 scenarios, the sensor initially scans the road for finding (detecting) a rear vehicle. This can be seen from the initial back and forth angular motion of the laser sensor shown on the right side of the figure for each scenario. Once the vehicle is detected, the angular motion of the laser sensor varies more gradually as it tracks the motion of the vehicle. The estimated longitudinal and lateral distances X and Y track the actual distances accurately throughout the vehicle motion in each scenario.

Note that good estimation leads to good prediction of the vehicle movement, and consequently good orientation control of the laser sensor. Achieving good orientation control of the laser sensor enables continuous future measurements from the corner of the vehicle.

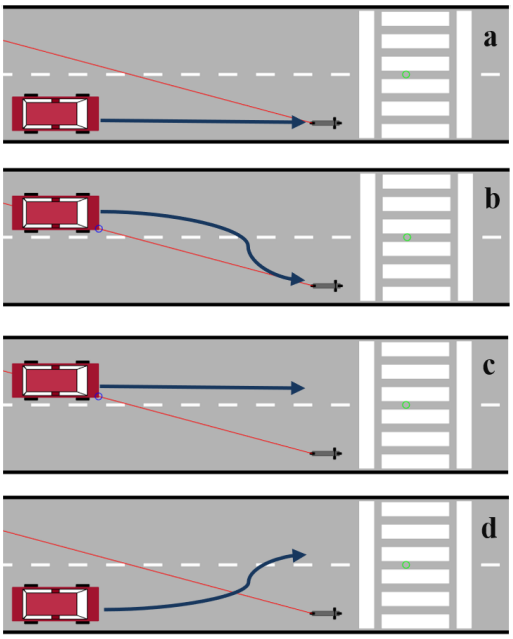

Fig. 5. Rear vehicle approaching scenarios considered in this paper. Four distinct scenarios are considered.

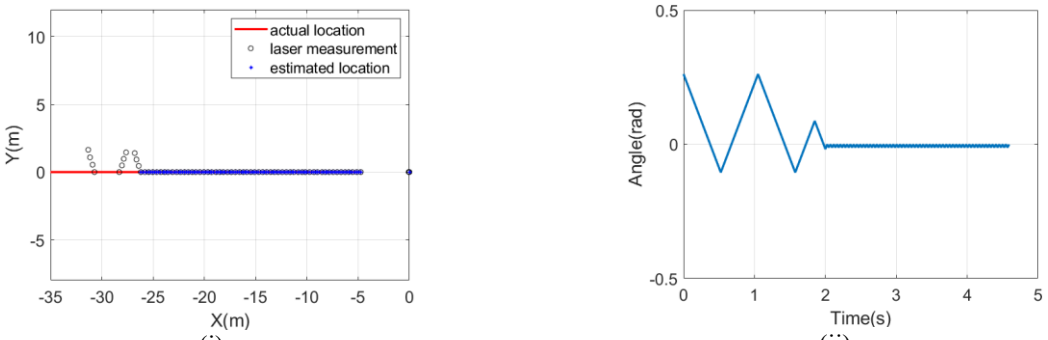

(i) (ii)

Scenario a: vehicle travels right behind scooter

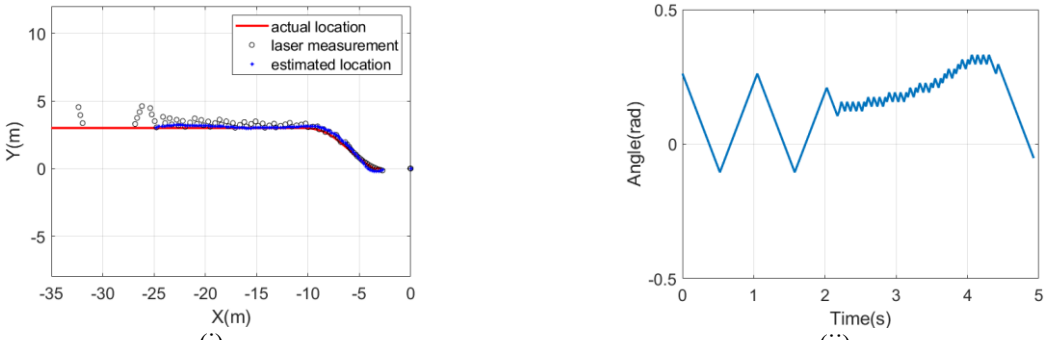

(i) (ii)

Scenario b: vehicle moves from adjacent lane to behind scooter

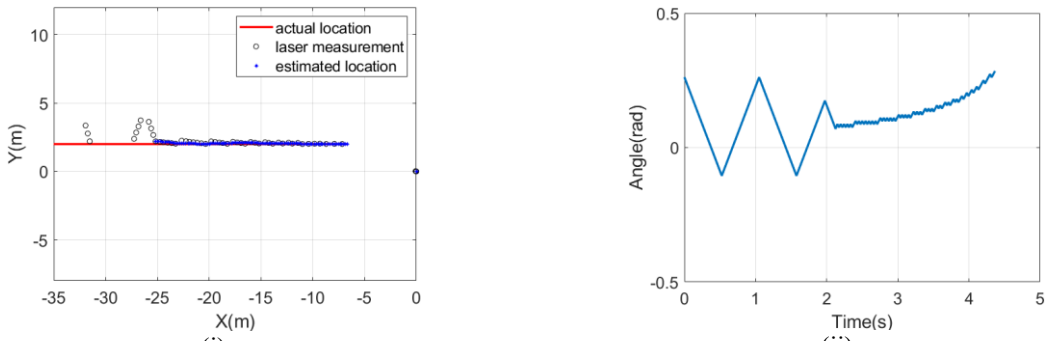

(i) (ii)

Scenario c: vehicle travels in adjacent lane

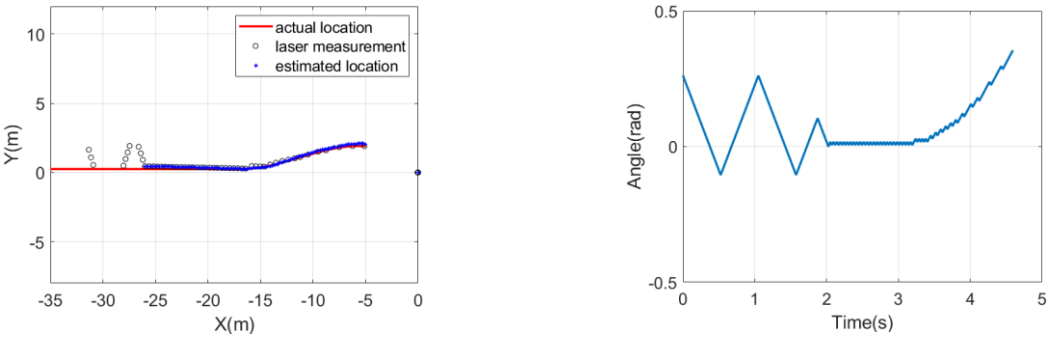

(i) (ii)

Scenario d: vehicle initially behind scooter changes lane to adjacent lane

Fig. 6. Simulation Results in MATLAB for 4 different scenarios. The vehicle maneuvers for the 4 scenarios are shown in Fig. 5. In each scenario, the lateral and longitudinal distances are shown in the left figure and the angular position of the laser sensor is shown in the right figure.

6.2. Experimental Results

First real-world experiments were conducted by riding the scooter on roads with regular traffic, primarily in the bicycle lane. More than two hours of real-time data with real-world traffic have been obtained and show the capability of the e-scooter system to perform reliably, track vehicles both behind and adjacent to the scooter, and provide minimal false alarms. Fig. 7 shows example results from riding in real-world traffic. In this data set, 3 consecutive vehicles pass by the scooter, one behind the other in rapid succession.

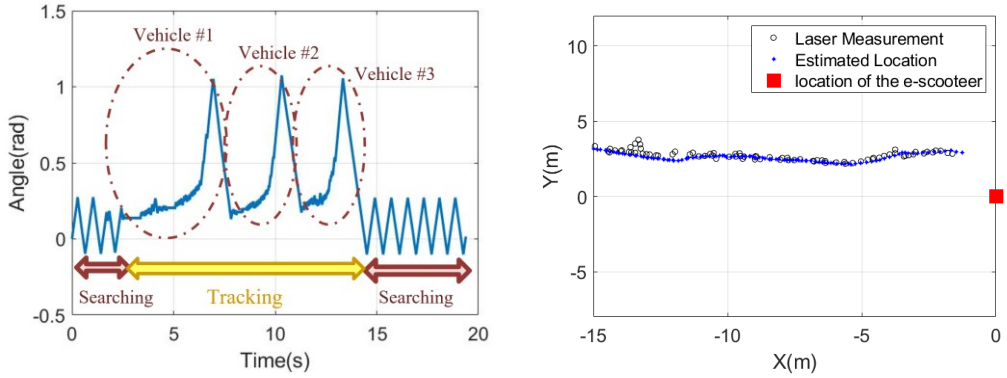

(i) **(ii)**

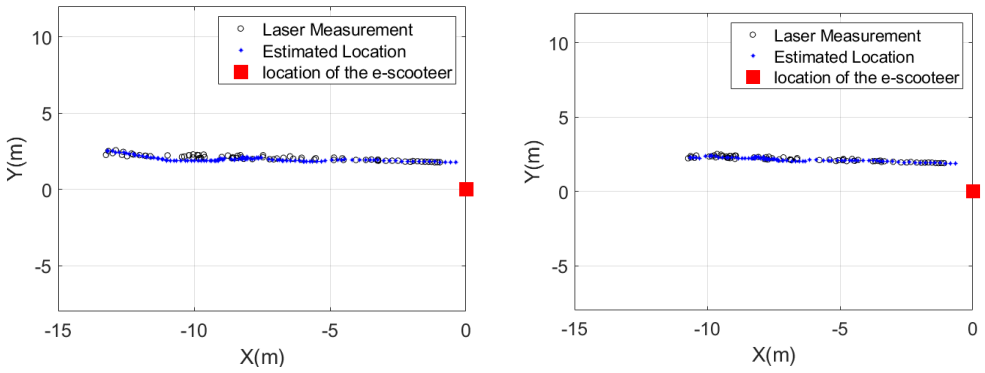

(iii) **(iv)**

Fig. 7. Experimental performance in real-world traffic: Tracking of 3 consecutive vehicles as they pass by e-scooter traveling in bicycle lane: **(i)** Scneraio c: Beam angle results from the active control system **(ii)** Vehicle #1: Lateral and longitudinal positions **(iii)** Vehicle #2: Lateral and longitudinal positions **(iv)** Vehicle #3: Lateral and longitudinal positions

Fig. 7 (i) shows the rotation angle of the laser sensor and how the active rotation control system is able to track all 3 vehicles, following them as they come closer and right next to the scooter, and then subsequently initiate detection and tracking of the next following vehicle. Figures 7 (ii), 7 (iii) and 7 (iv) show the individual estimated trajectories in terms of lateral and longitudinal positions of the three individual vehicles. When the sensor stops tracking each vehicle, the maximum angle of the laser sensor is around 1 radian and the longitudinal distance is typically less than 1 meter.

Since riding in regular real-world traffic for a couple of hours does not necessarily put the scooter in danger, we conducted special experiments using our own cars which operate with controlled maneuvers that pose potential danger to the rider, triggering an audio alarm from the e-scooter. These experiments are for scenario a and scenario b, which are scenarios that could potentially result in a situation involving the possibility of a car-scooter collision. In order to perform these experiments safely, a stand was designed to position the scooter by itself without requiring the rider to be present, as shown in Fig. 8. In scenario a, the vehicle drives behind the e-scooter and stops in a dangerous manner just behind the e-scooter. As shown in Fig. 9 (Scenario a), the system can track the vehicle correctly from 25 meters away. Scenario d on the other hand is the more complicated case in which the vehicle initially drives behind the e-scooter, and then changes lanes to pass by in a safely manner. As shown in Fig. 9 (Scenario d), the system has been able to track two different vehicles and track them accurately.

While scenarios a-d are the most likely maneuvers to be encountered in regular e-scooter riding on local roads, we also tested the ability of the active tracking system to track vehicles during some unusual vehicle maneuvers involving multiple lane changes. Performances during these complicated vehicle trajectories are shown in Fig. 10. The first and second scenarios include weaving behind the e-scooter involving two lane changes by the rear vehicle. In Fig. 10 (i) the vehicle changes to come behind the e-scooter and then changes lanes again after receiving an audio honk from the e-scooter. In Fig. 10 (ii) the vehicle changes lanes multiple times and ends up stopping just behind the e-scooter. In the third scenario in Fig. 10 (iii), the vehicle makes a sudden lane change from a large lateral distance and suddenly moves directly towards the e-scooter. All three unusual scenarios could result in a situation involving the possibility of a car-scooter collision depending on the relative trajectories of the car and e-scooter.

Fig. 8. Scenario d experiments with the e-scooter setup on a stand in order to avoid danger to a human subject in these risky experiments. In these specific experiments, the vehicle is initially behind the e-scooter and then changes lane in response to an audio warning by the scooter.

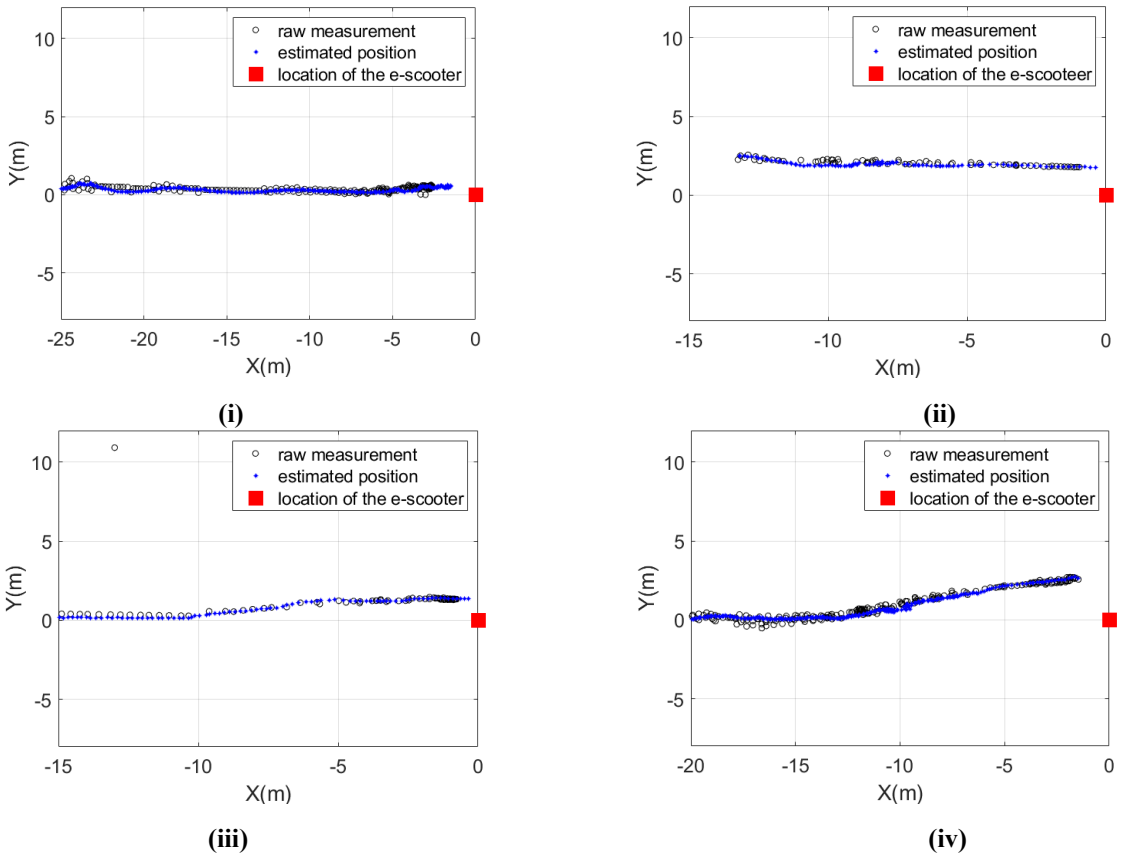

Fig. 9. Experimental results for typical vehicle maneuvers encountered. **(i)** Scenario a: Vehicle right behind scooter **(ii)** Scenario c: Vehicle travelling in adjacent lane **(iii)** Scenario d: Vehicle initially behind scooter changes lane **(iv)** Scenario d: Vehicle behind scooter suddenly changes lane

It should be noted here that a car horn audio might not be the optimal audio for this warning situation – A better auditory warning signal that is effective at alerting other cars could be determined through a human factors study for this e-scooter application.

We also compared the performance of the new nonlinear observer with the performance of an interacting multiple-model (IMM) algorithm previously used in vehicle tracking [32]. The IMM algorithm utilizes two models for the vehicle – straight driving and constant rate turning – processing them simultaneously but switching between the two models according to their updated weights [32], [33]. The IMM algorithm has been used significantly for vehicle tracking in both aerospace and ground vehicle applications. The experimental results in Fig. 11 show data for a vehicle with varying velocity that travels right behind the e-scooter and then changes lanes after getting close. The results in Fig. 11 suggest that the IMM EKF algorithm with time-varying observer gain and the new nonlinear observer have almost the same performance, except towards the final time portion of the data shown where the nonlinear observer seems to work better. The IMM filter requires significantly more computation, since it must process two models simultaneously and calculate the filter gains and model weights in real-time. Also, the IMM filter is based on linearization and has no rigorous proof of stability for nonlinear models. The nonlinear observer has the advantages of global stability, easy implementation, and can estimate the states directly using a single constant observer gain.

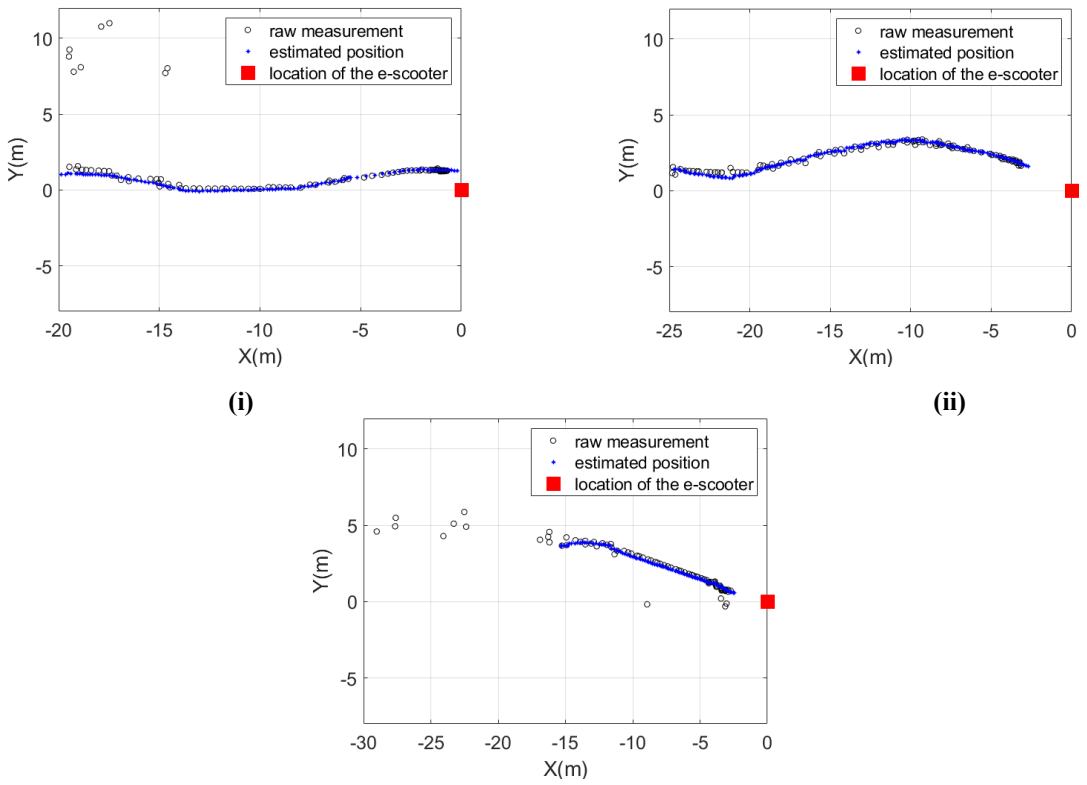

Fig. 10. Estimation results of the observer in scenarios with unusual vehicle trajectories involving lane changes. **(i)** Extra scenario involving multiple lane changes **(ii)** Extra weaving scenario with multiple lane changes **(iii)** Extra scenario involving sudden lane change from large lateral distance

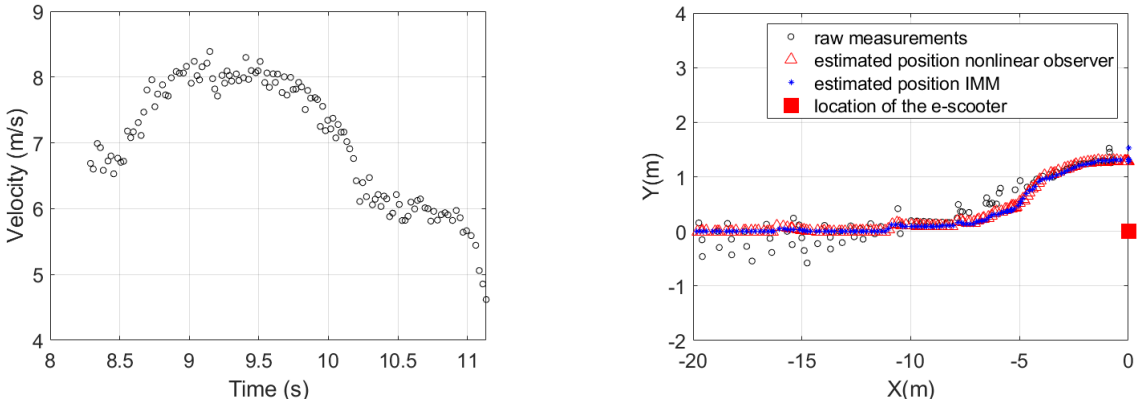

Fig. 11. Comparing the IMM EKF and the new nonlinear observer in an experiment with variable velocity

For further analysis, the time-to-collision (TTC) for a vehicle approaching the e-scooter with various initial speeds from the rear is shown in Fig. 12. In this example, it is assumed that the vehicle is only detected by the system when it is 30 meters away from the e-scooter. The convergence time of the observer is 0.45 seconds (based on simulations and experiments), and the driver's reaction time is assumed to be 0.9 seconds. The collision warning system will be effective in cases in which the vehicle has a speed of less than 50 mph, making it suitable for local roads. For speeds above 20 mph, the vehicle driver will be able to

avoid the accident only by steering, while the driver can also avoid the accident purely by braking and slowing down for speeds below 20 mph. To increase the safety of the collision warning system for higher speed values (e.g., on high-speed roads) the laser sensor should have a higher range and the stepper motor should have a better resolution, such that the initial detection range increases.

Recognizing that the actual corner of a vehicle is rounded, accurately tracking the corner-most point of the vehicle is challenging. Errors in tracking the corner-most point in the presence of a curvature on the corner will result in errors in longitudinal and lateral position estimation. The maximum error can occur in either longitudinal or lateral distance and will depend both on the magnitude of error in tracking the corner-most point and the angle of the line connecting the measurement point to the corner-most point. The position error is analyzed in Figure 13 and shows that the error remains small (of the order of centimeters) for even large angle deviations due to rounding of the corner.

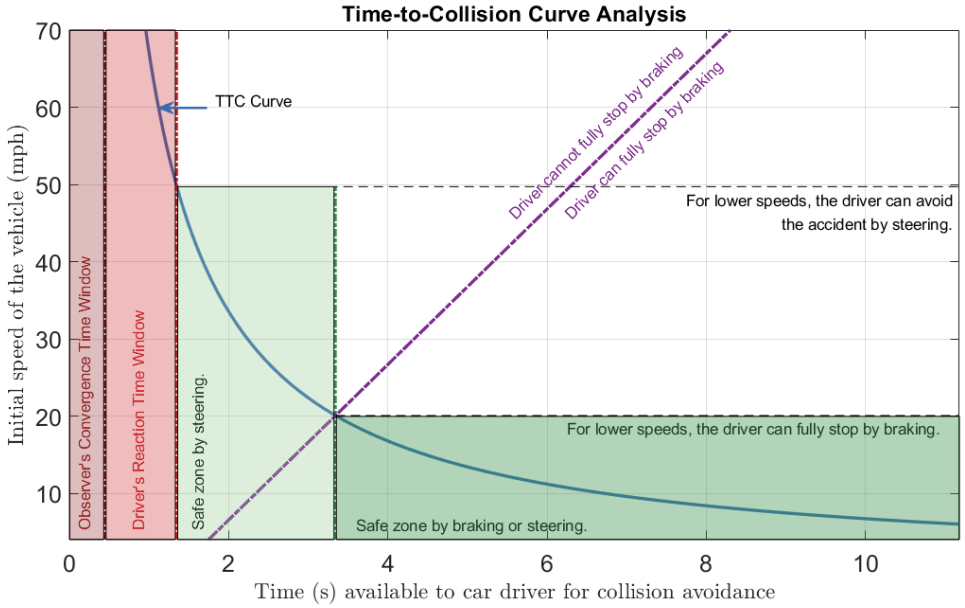

Fig. 12. Time-to-collision for a vehicle detected 30 meters away and approaching right behind the e-scooter with a constant speed. The vehicle driver can avoid the accident purely by braking only if the initial speed is approximately below 20 mph. The vehicle driver can avoid the accident by steering away from behind the e-scooter if the initial speed is approximately below 50 mph. The results suggest that the proposed system will be effective on local roads.

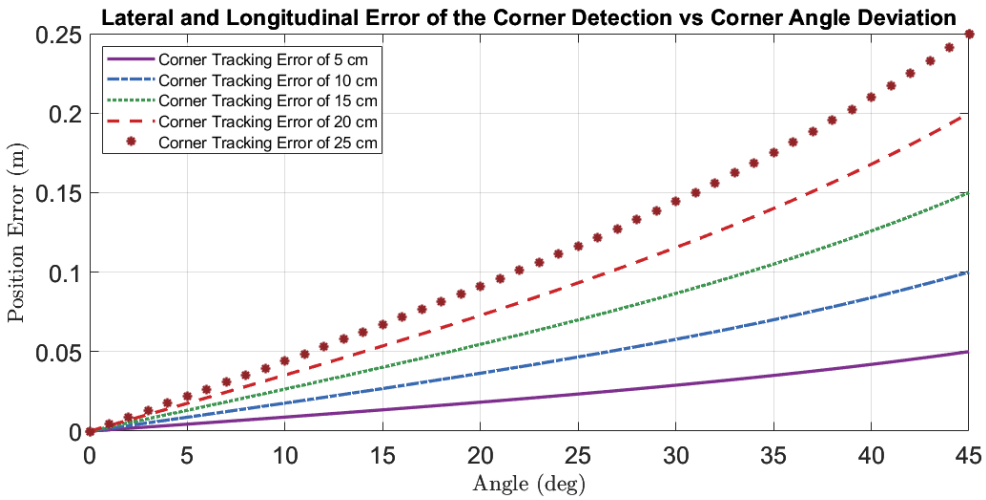

Fig. 13. The effect of the corner angle deviation from 90 degrees on the maximum longitudinal or lateral position error.

7. Conclusion

An active sensing system for protection of an e-scooter from car-scooter collisions is developed in this paper. The performance of this system is evaluated both in simulations and experiments. A low-cost single-beam laser sensor is chosen for measuring the positions of cars behind the scooter. The sensor is mounted on a stepper motor and the region behind the scooter is scanned to detect vehicles. Once a vehicle is detected, its trajectory is tracked in real-time by using feedback control to focus the orientation of the laser sensor such as to make measurements of the right front corner of the vehicle. A nonlinear vehicle model and a nonlinear observer are used to estimate the trajectory variables of the tracked car. The estimated states are used in a receding horizon controller that controls the real-time position of the laser sensor to focus on the vehicle. The active sensing system tracks the trajectories of cars in order to predict any real-time danger of collision. Extensive experimental results both in regular real world traffic and in special experiments conducted by the research team to put the e-scooter in a dangerous near-collision scenario were presented. The experimental results verify that the developed system works reliably and can accurately track trajectories of rear vehicles in all the scenarios considered. A limitation of the developed system is that it tracks only one rear vehicle at a time. Tracking multiple vehicles requires both fast measurement frequency and large measurement range and was not considered in this paper.

Future work in the domain of e-scooter rider protection can include consideration of other types of crashes besides rear vehicle crashes, for example vehicles at an upcoming traffic intersection which might potentially pose a frontal/side collision danger to the e-scooter. Another aspect of improving safety for other road users could include monitoring of any danger posed to pedestrians by the e-scooter and corresponding warnings to the e-scooter rider.

From a policy recommendations perspective, preventing scooters from riding on sidewalks (to protect pedestrians) and allowing e-scooters to use bicycle lanes could be mandated by cities and states. Large-scale field tests of safety systems for preventing vehicle-scooter collisions need to be conducted. This could be followed by mandating the type of vehicle-scooter collision warning system developed in this paper to be used on all e-scooters.

Acknowledgments

This research was supported in part by a research grant from the National Science Foundation (NSF Grant CPS 2038403).

8. References

[1] Grand View Research, "Electric Scooters Market Size, Share & Trends Analysis Report", 2020 – 2030, Report ID: GVR-1-68038-196-2, February 2020.

[2] Voro Motors, "Rules and Regulations of Electric Scooter in Different Countries," Online article, Accessed on May 11, 2023, https://www.voromotors.com/blogs/news/rules-and-regulations-of-electric-scooter-in-different-countries

[3] Unagi, "Comprehensive Guide to Electric Scooter Laws 2022," Online article, Accessed on May 11, 2023, Available at: https://unagiscooters.com/scooter-articles/the-comprehensive-guide-to-electric-scooter-laws-2022/

[4] Wruck Paupore, "State by State Guide to Scooter Laws in 2023," Online resource, https://www.wp-law.com/state-by-state-guide-to-scooter-laws-in-2023/, Accessed on January 9, 2023.

[5] T. K. Trivedi, C. Liu, A. L. M. Antonio, N. Wheaton, V. Kreger, A. Yap, D. Schriger and J. G. Elmore, "Injuries Associated with Standing Electric Scooter Use", JAMA Network Open. 2019; Vol. 2, No. 1, e187381, 2019.

[6] Niemann, M., Braun, K.F., Otto, E., Tiefenbrunner, M., Wüster, J., Stöckle, U., Ahmad, S.S., Märdian, S. and Graef, F., 2023. Dangers of e-mobility: a systematic review and meta-analysis of sustained injury patterns and injury severity. Safety science, 167, p.106283.

[7] T. K. Trivedi, C. Liu, A. L. M. Antonio, N. Wheaton, V. Kreger, A. Yap, and J. G. Elmore, (2019), "Injuries associated with standing electric scooter use". JAMA network open, 2(1), e187381-e187381.

[8] A. Griswold (2020, Feb.). "At least 29 people have died in electric scooter crashes since 2018". Quartz.com. Retrieved from: https://qz.com/1793164/at-least-29-people-have-died-in-electric-scooter-crashes/

[9] E. Karpinski, E. Bayles, L. Daigle, D. Mantine, "Comparison of motor-vehicle involved e-scooter fatalities with other traffic fatalities," *Journal of Safety Research*, Vol. 84, pp. 61-73, 2023.

[10] James A, Harrois A, Abback P, et al. Comparison of Injuries Associated With Electric Scooters, Motorbikes, and Bicycles in France, 2019-2022. *JAMA Netw Open.* 2023;6(6):e2320960. doi:10.1001/jamanetworkopen.2023.20960

[11] J. Tark, "Micromobility Products-Related Deaths, Injuries, and Hazard Patterns: 2017–2021," United States Consumer Product Safety Commission Report, September 2023.

[12] Y. K. Liew, C. P. J. Wee and J. H. Pek, "New peril on our roads: a retrospective study of electric scooter-related injuries", Singapore Med J, Vol. 61, No. 2, pp. 92-95, 2020.

[13] Henri Vasara, Linda Toppari, Veli-Pekka Harjola, Kaisa Virtanen, Maaret Castrén & Arja Kobylin, "Characteristics and costs of electric scooter injuries in Helsinki: a retrospective cohort study," Scandinavian Journal of Trauma, Resuscitation and Emergency Medicine, Vol. 30, Article number: 57, November 2022.

[14] Bekhit MNZ, le Fevre J, Bergin CJ, "Regional healthcare costs and burden of injury associated with electric scooters," *Injury*, Vol. 51, No. 2, pp. 271–7, Feb 2020.

[15] Lavoie-Gagne O, Siow M, Harkin WE, Flores AR, Politzer CS, Mitchell BC, "Financial impact of electric scooters: a review of injuries over 27 months at an urban level 1 trauma center," *Trauma Surgery and Acute Care Open*, Vol. 6, No. 1, 2021.

[16] MacAlister, A. and Zuby, D.S., 2015, March. Cyclist crash scenarios and factors relevant to the design of cyclist detection systems. In 2015 IRCOBI Conference Proceedings-International Research Council on the Biomechanics of Injury (pp. 373-384).

[17] K. McLeod and L. Murphy, "Every bicyclist counts", League of American Bicyclists, Report, May 2014.

[18] Ziebinski, A., Cupek, R., Erdogan, H., Waechter, S. (2016), "A Survey of ADAS Technologies for the Future Perspective of Sensor Fusion," In: Nguyen, N., Iliadis, L., Manolopoulos, Y., Trawiński, B. (eds) Computational Collective Intelligence. ICCCI 2016. Lecture Notes in Computer Science, vol 9876, Springer, 2016.

[19] Tabitha S. Combs, Laura S. Sandt, Michael P. Clamann, Noreen C. McDonald, "Automated Vehicles and Pedestrian Safety: Exploring the Promise and Limits of Pedestrian Detection, American Journal of Preventive Medicine, Volume 56, Issue 1, pp. 1-7, 2019.

[20] S. B. Eisenman, E. Miluzzo, N. D. Lane, R. A. Peterson, G-S. Ahn, and A. T. Campbell, "The BikeNet mobile sensing system for cyclist experience mapping," in 5th ACM Conference on Embeded Networked Sensor Systems (SenSys 2007), Sydney, Australia, 2007, pp. 87 - 101.

[21] S. Smaldone, C. Tonde, V. K. Ananthanarayanan, A. Elgammal, and L. Iftode, "The cyber-physical bike: a step towards safer green transportation," In 12th Workshop on Mobile Computing Systems and Applications, Phoenix, AZ, 2011, pp. 56 – 61.

[22] Northeastern University. (2014, Jan. 21). Northeastern students develop 'Smart Bike' tech to curb cycling death [Online]. Available at: http://www.bizjournals.com/boston/blog/startups/2014/01/northeastern-students-develop-smart.html.

[23] Garmin. Varia Rearview Radar. Accessed: Jan. 26, 2019. [Online]. Available: https://buy.garmin.com/en-US/US/p/518151

[24] W. Jeon and R. Rajamani, "Rear vehicle tracking on a bicycle using active sensor orientation control." IEEE Transactions on Intelligent Transportation Systems, Vol. 19, No. 8, pp. 2638-2649, 2017.

[25] K. M. Jensen, I. F. Santos, L. K.H. Clemmensen, S. Theodorsen, H. J.P. Corstens, "Mass estimation of ground vehicles based on longitudinal dynamics using loosely coupled integrated navigation system and CAN-bus data with model parameter estimation," Mechanical Systems and Signal Processing, Volume 171, 2022.

[26] A. J. Rodríguez, E. Sanjurjo, R. Pastorino, M. Á. Naya, "State, parameter and input observers based on multibody models and Kalman filters for vehicle dynamics," Mechanical Systems and Signal Processing, Volume 155, 2021.

[27] S. Rafatnia, M. Mirzaei, "Estimation of reliable vehicle dynamic model using IMU/GNSS data fusion for stability controller design," Mechanical Systems and Signal Processing, Volume 168, 2022.

[28] Yicai Liu, Lingtao Wei, Zhixian Fan, Xiangyu Wang, Liang Li, “Road slope estimation based on acceleration adaptive interactive multiple model algorithm for commercial vehicles,” Mechanical Systems and Signal Processing, Volume 184, 2023.

[29] M. Ester, H. P. Kriegel, J. Sander and X. Xu, "A density-based algorithm for discovering clusters in large spatial databases with noise", KDD, vol. 96, no. 34, pp. 49-60, Aug. 1996.

[30] R. Rajamani, “Vehicle dynamics and control”. Springer Science & Business Media, 2011.

[31] S. Boyd, L. El Ghaoui, E. Feron and V. Balakrishnan. “Linear Matrix Inequalities in System and Control Theory”. SIAM Studies in Applied Mathematics. SIAM, Philadelphia, Pennsylvania, 1994.

[32] Y. Bar-Shalom, X. R. Li, and T. Kirubarajan, Estimation with Applications to Tracking and Navigation: Theory Algorithms and Software, Hoboken, NJ, USA: Wiley, 2004.

[33] P. Xu, L. Xiong, D. Zeng, Z. Deng and Z. Li, "IMM-KF Algorithm for Multitarget Tracking of On-Road Vehicle," SAE Technical Paper 2020-01-0117, 2020, https://doi.org/10.4271/2020-01-0117.

[34] R. Rajamani, W. Jeon, H. Movahedi and A. Zemouche, “On the need for switched-gain observers for non-monotonic nonlinear systems”. Automatica, Volume 114, 2020.